ISTITUTO NAZIONALE DI FISICA NUCLEARE

INFN/TC-82/10
19 Luglio 1982

E. Fabrici: MAGNETIC FORCES ON THE COILS OF THE SUPERCONDUCTING CYCLOTRON AT THE UNIVERSITY OF MILAN

Servizio Documentazione
dei Laboratori Nazionali di Frascati

Istituto Nazionale di Fisica Nucleare
Sezione di Milano

INFN/TC-82/10
19 Luglio 1982

MAGNETIC FORCES ON THE COILS OF THE SUPERCONDUCTING CYCLOTRON AT THE UNIVERSITY OF MILAN

E. Fabrici
Università degli Studi di Milano, and INFN - Sezione di Milano

1. - INTRODUCTION.

A three sectors cyclotron with superconducting coils is now under construction at the University of Milan. The machine covers a wide range of energies and ions, the maximum design energies being 100 MeV/n for fully stripped light ions and 20 MeV/n for the heaviest ones, corresponding to a K_{foc} equal to 200 MeV and K_b equal to 800 MeV respectively. The machine design and the expected performances are presented in detail in Ref. (1). An important issue in designing superconducting coils for a cyclotron is to estimate with some accuracy the forces acting on them, in particular those arising from centering errors etc. These calculations are usually plagued by a number of uncertainties. Some effort has been made in order to narrow down the errors limits, and this paper reports briefly on the results. They concern:

a) The axial forces arising in an ideal situation, i. e. when the coils are perfectly centered with respect to the iron structure.
b) The axial and radial forces arising from errors in the coils positioning.

Since the coils design is extensively described in Ref. (2), it is sufficient to recall these aspects:

- the coils are split into two independently excited sections in order to achieve the proper

isochronism for all the ions, while minimising the necessary trim-coil power. The section closer to the median plane is referred to in the following as coil α, the one farther away as coil β. A sketch of the coils geometry with all the relevant dimensions is given in Fig. 1.

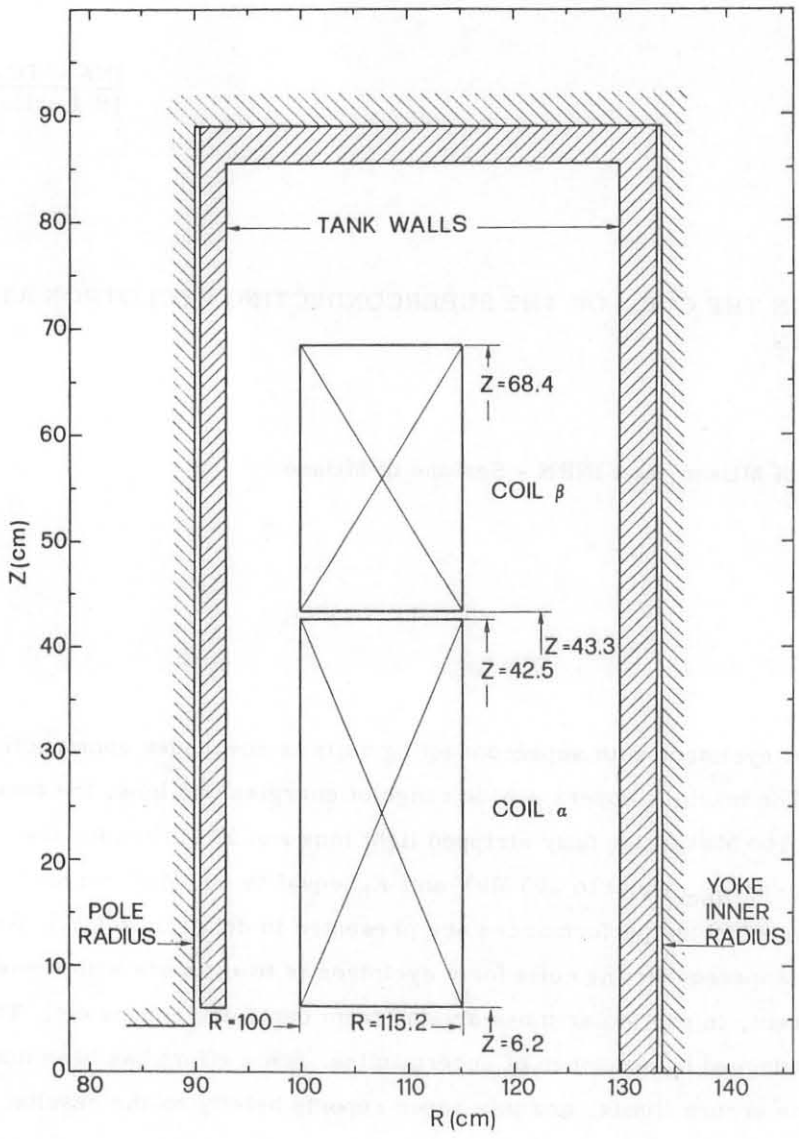

FIG. 1 - Schematic cross section of the coils. All the dimensions are in cm.

- The coils are wound with the double pancake technique and the pancakes are held together with properly prestressed rods so that, from a mechanical point of view, the ensemble of the coils above and below the median plane can be regarded as a rigid body. The coils are supposed perfectly cylindrical with a uniform current density equal to the actual average current density.

The operating diagram of the cyclotron in the (I_α, I_β) plane is given in Fig. 2. The average current densities J_α and J_β, are given by the upper and right scale in A/cm^2. On the diagram lines of constant center field, B_o, and charge to mass ratio, Z/A, are also shown. The current densities range between 1500 and 3500 A/cm^2 in the α section and between - 1500 and + 3500 A/cm^2 in the β section, the minus sign meaning that the currents are opposite in the two sections. For accelerating $^3He^{++}$ beams the negative limit J_β may reach - 2000 A/cm^2.

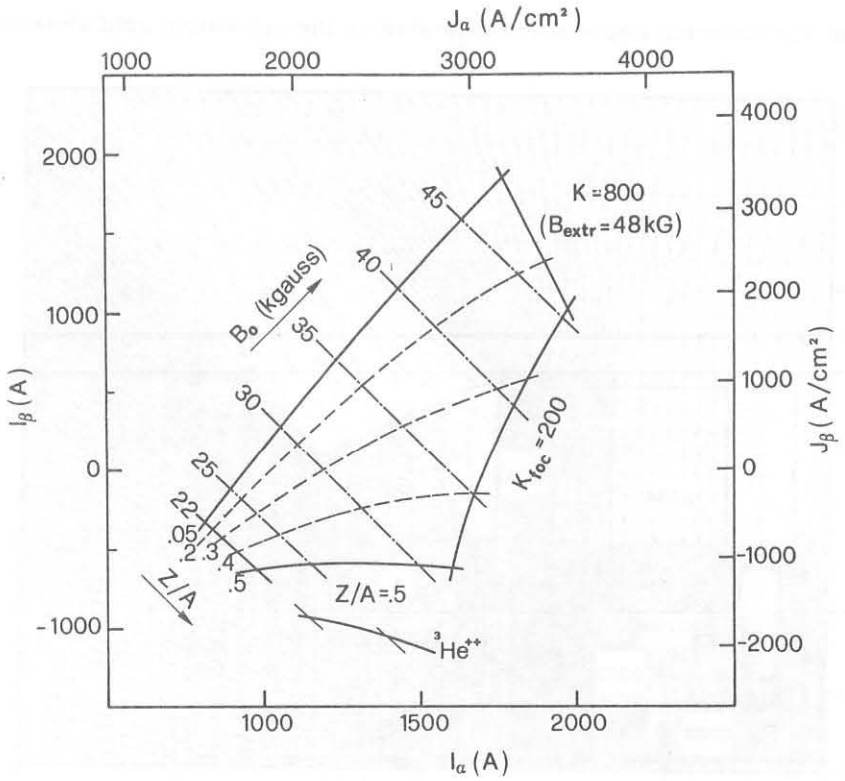

FIG. 2 - Operating diagram of the cyclotron in the (I_α, I_β) plane. The average current densities are given by the right and upper scale.

The magnetic forces have been calculated by integrating the expression $\underline{dF} = i \cdot \underline{dl} \wedge \underline{B}$ over the coil region. The fields have been calculated using the magnetostatic bidimensional code POISCR[3], a modifed version of the POISSON program which computes the vector potential over a relaxation grid consisting of 6000 points at maximum. The magnetic properties can be defined with up to ten different B-H tables.

2. - POISCR CALCULATIONS.

The circular parts of the magnet exhibiting cylindrical symmetry such as the overall yoke structure and the coils are treated exactly. Following the TRIM models adopted at

M. S. U.[4], different B-H tables have been adopted in order to describe with iron rings of different magnetization all the elements not having cylindrical symmetry like the sectors, the holes through the upper part of the yoke and the poles, and the penetrations through the yoke median plane necessary for beam injection and extraction etc. For these non symmetric regions the field B has been scaled assuming that the iron magnetization M is reduced according to $\underline{B} = \mu_o \underline{H} + F \cdot \underline{M}$. In this formula the fraction F is the ratio between the actual volume of the iron and the volume of the circular ring which simulates it. The iron fractions used for the different regions are indicated on the relaxation grid shown on Fig. 3.

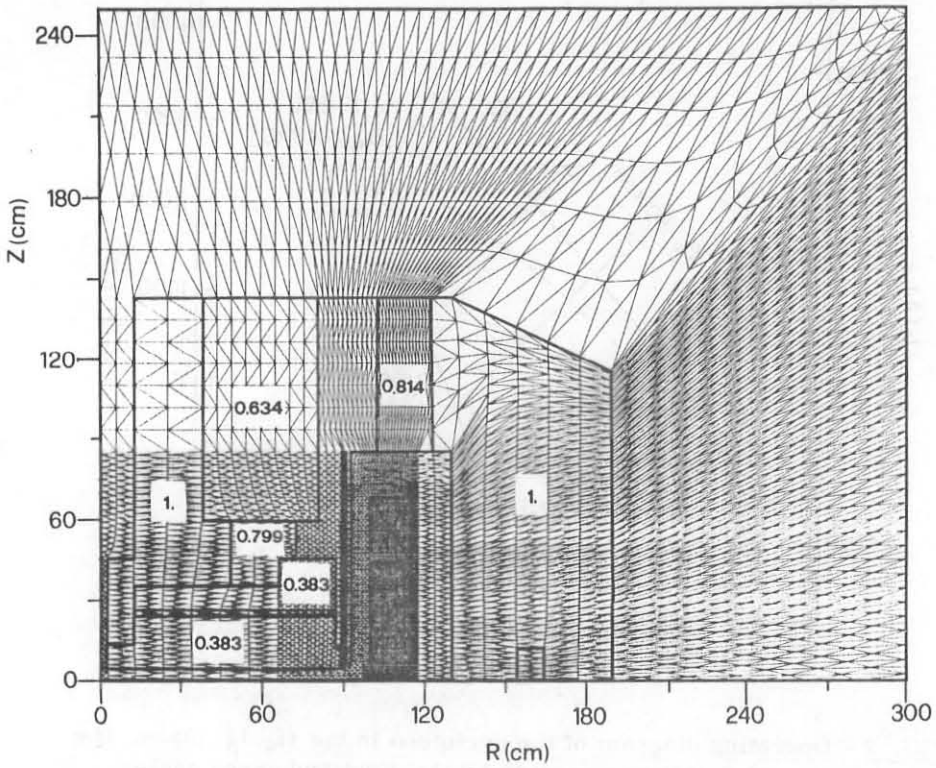

FIG. 3 - Relaxation grid used for the magnetic field calculations with the POISCR code. The numbers over the iron regions show the iron fraction, F, used (see text for details).

The grid has been chosen so as to give the highest points density in the coils regions. It has been checked that the field on the median plane agrees within 100 Gauss for $r \gtrsim \sim 20$ cm with the one obtained using the relaxation grid optimized for median plane calculations[5]. Lines of constant flux are shown, together with the regions subdivisions, in Figs. 4 and 5 for the cases $J_\alpha = J_\beta = 3500$ A/cm^2 and $J_\alpha = 3000$, $J_\beta = -1500$ A/cm^2 respectively. These two limiting cases correspond respectively to the maximum ampere turns in the coils and to the maximum negative current in the β coils. Moreover, as can be seen from the operating diagram presented in Fig. 2, the former case is close to the bending limit of the machine and

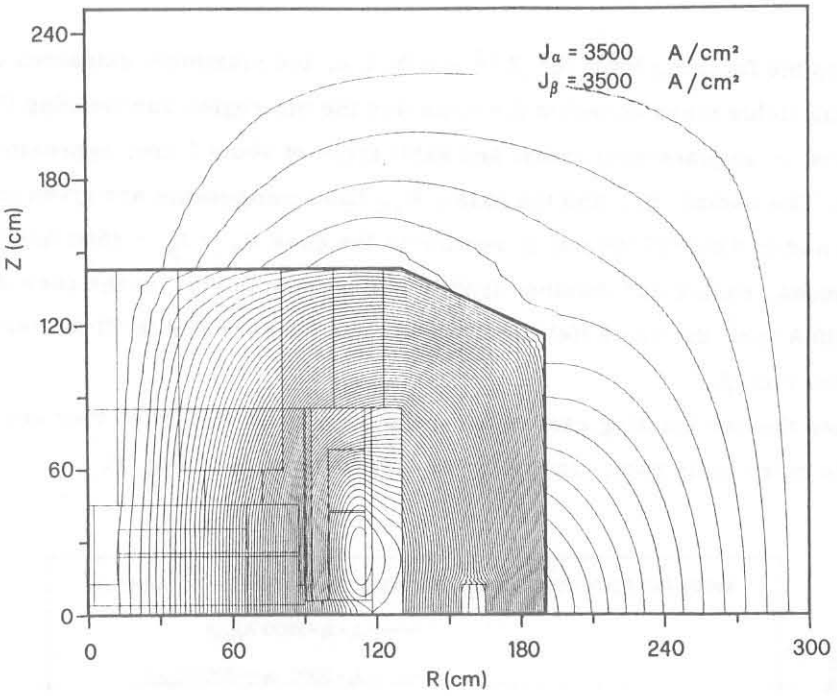

FIG. 4 - Lines of constant flux calculated by the POISCR code for the case $J_\alpha = J_\beta = 3500$ A/cm^2.

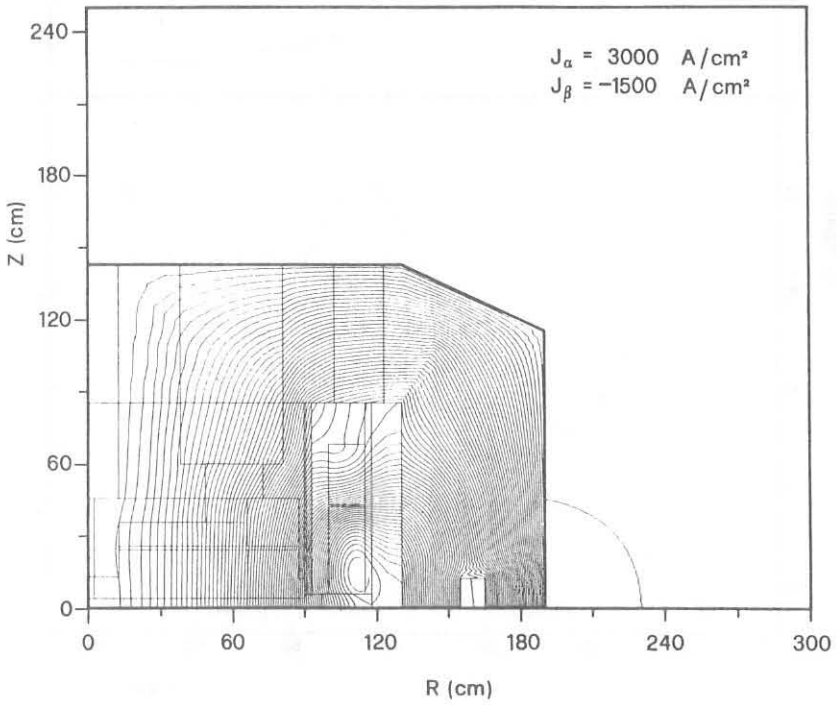

FIG. 5 - Lines of constant flux calculated by the POISCR code for the case $J_\alpha = 3000$, $J_\beta = -1500$ A/cm^2.

the latter one to the focusing limit for $Z/A = 0.5$, i. e. the maximum extracted energy.

Magnetic fields maps covering the coils and the air region surrounding them have been calculated in the (r, z) plane with radial and axial steps of about 1 cm, approximately equal to the mesh size. The radial, B_r, and the axial, B_z, field components are given in Table I for the α section and in Table II for the β section in the case $J_\alpha = J_\beta = 3500\ A/cm^2$. Field values are in Kgauss, radius and distance from median plane in cm. In the case $J_\alpha = 3000\ A/cm^2$ and $J_\beta = -1500\ A/cm^2$ the same field components are listed in Table III for the coil α and in Table IV for the coil β.

For both the two limiting cases, the trend of B_z and B_r, when they are averaged from the inner to the outer coils radii, is plotted as a function of z in Fig. 6.

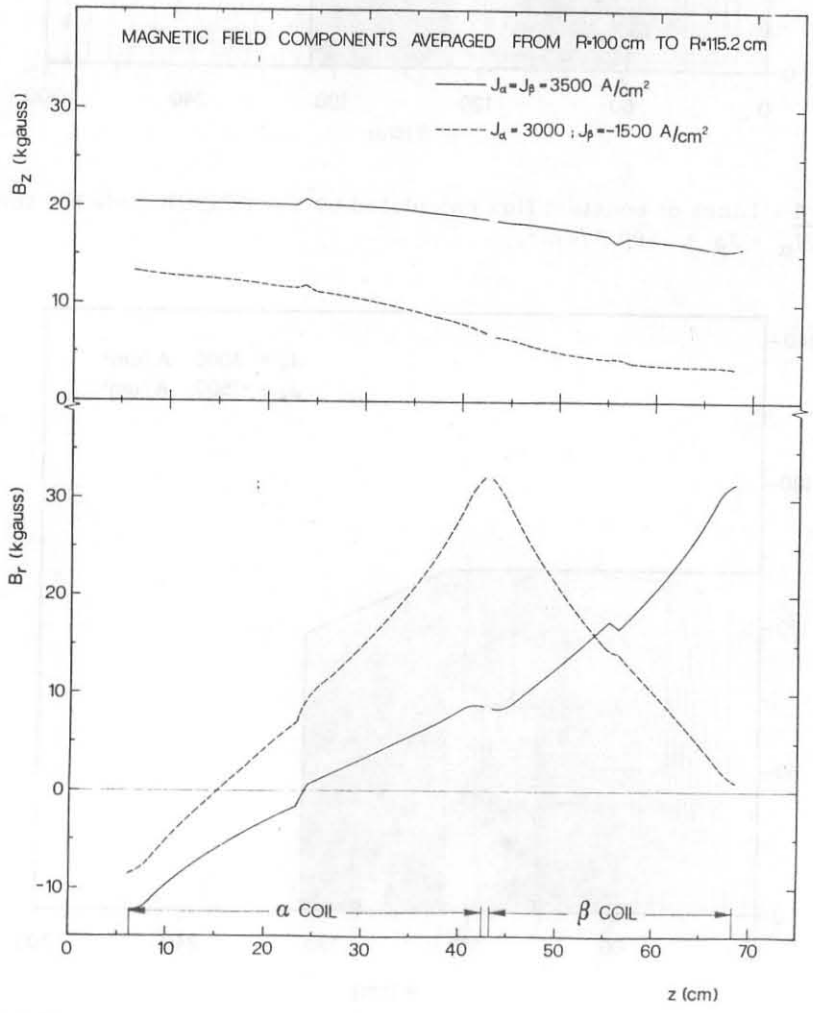

FIG. 6 - Axial, B_z, and radial, B_r, field components inside the coils. The field components are averaged from the inner to the outer coils radii and plotted as a function of z. The solid lines refer to the $J_\alpha = J_\beta = 3500\ A/cm^2$ case, while the dashed ones to the $J_\alpha = 3000$, $J_\beta = -1500\ A/cm^2$ case.

TABLE I

COIL ALPHA AT 3500.00 AZ(CM*CM) COIL BETA AT 3510.00 AZ(CM*CM)

BZ (KGAUSS)
BR (KGAUSS) COIL ALPHA

Z(cm)	100.0	101.0	102.0	103.0	104.1	105.1	106.1	107.1	108.1	109.1	110.1	111.1	112.2	113.2	114.2	115.2	Z(cm)
42.5	44.48 7.97	42.71 8.16	34.55 8.15	35.44 8.51	32.27 8.83	29.57 8.71	26.86 8.80	24.14 8.86	21.41 8.90	18.64 8.92	9.97 8.93	6.27 8.91	2.59 8.88	-1.03 8.81	-4.47 8.67	-6.92 8.57	42.5
41.5	44.78 7.79	42.27 8.14	38.42 8.50	35.14 8.72	31.43 8.87	27.71 9.00	23.97 9.07	20.23 9.13	16.49 9.17	12.75 9.19	9.01 9.19	5.28 9.16	1.57 9.10	-2.10 8.98	-5.31 8.80	-7.50 8.60	41.5
40.5	45.40 7.44	43.70 7.87	40.37 8.14	36.63 8.40	32.48 8.57	28.12 8.69	25.36 8.79	21.59 8.85	17.82 8.89	14.06 8.90	10.29 8.89	6.53 8.86	2.77 8.79	-.99 8.67	-4.57 8.48	-7.09 8.21	40.5
39.5	45.62 7.01	42.96 7.30	39.36 7.57	35.55 7.77	31.76 7.93	27.47 8.05	24.19 8.14	20.39 8.21	16.59 8.25	12.81 8.27	9.02 8.26	5.23 8.22	1.43 8.15	-2.36 8.05	-5.67 7.87	-7.90 7.64	39.5
38.5	46.55 6.43	44.38 6.74	40.96 7.02	37.14 7.20	33.30 7.35	29.47 7.47	25.66 7.56	21.84 7.62	18.03 7.66	14.21 7.68	10.39 7.67	6.57 7.64	2.75 7.58	-1.09 7.49	-4.78 7.37	-7.35 7.17	38.5
37.5	46.25 6.03	43.55 6.28	39.89 6.49	36.02 6.64	32.16 6.74	28.32 6.82	24.47 6.87	20.64 7.03	16.80 7.07	12.96 7.09	9.12 7.09	5.28 7.07	1.42 7.02	-2.43 6.95	-5.80 6.81	-8.07 6.61	37.5
36.4	47.09 5.47	44.38 5.80	41.42 5.99	37.54 6.13	33.66 6.25	29.79 6.35	25.92 6.43	22.06 6.49	18.21 6.52	14.35 6.55	10.49 6.55	6.62 6.53	2.75 6.49	-1.14 6.44	-4.86 6.35	-7.47 6.18	36.4
35.4	46.72 5.10	44.00 5.33	40.31 5.50	36.40 5.62	32.50 5.73	28.61 5.82	24.73 5.89	20.85 5.95	16.98 5.99	13.10 6.01	9.22 6.01	5.34 6.00	1.45 5.98	-2.44 5.94	-5.84 5.81	-8.15 5.62	35.4
34.4	47.50 4.54	45.26 4.67	41.74 5.03	37.87 5.14	33.99 5.23	30.09 5.31	26.15 5.38	22.26 5.43	18.37 5.47	14.44 5.49	10.58 5.50	6.69 5.50	2.78 5.48	-1.14 5.45	-4.89 5.39	-7.51 5.22	34.4
33.4	47.08 4.21	44.34 4.42	40.63 4.57	36.70 4.68	32.77 4.76	28.85 4.81	24.94 4.88	21.04 4.92	17.13 4.96	13.23 4.99	9.32 5.00	5.41 5.00	1.50 5.00	-2.41 4.98	-5.84 4.87	-8.16 4.66	33.4
32.4	47.81 3.63	45.55 3.97	42.05 4.11	38.12 4.19	34.19 4.26	30.26 4.33	26.34 4.34	22.42 4.43	18.51 4.46	14.59 4.49	10.68 4.51	6.75 4.52	2.83 4.52	-1.10 4.51	-4.87 4.47	-7.51 4.28	32.4
31.4	47.35 3.33	44.60 3.54	40.87 3.67	36.92 3.76	32.98 3.80	29.05 3.86	25.12 3.91	21.19 3.95	17.27 3.98	13.35 4.01	9.42 4.03	5.50 4.05	1.56 4.06	-2.36 4.06	-5.81 3.94	-8.14 3.72	31.4
30.4	48.03 2.75	45.75 3.10	42.24 3.22	38.31 3.28	34.36 3.33	30.42 3.39	26.49 3.42	22.56 3.46	18.63 3.50	14.70 3.53	10.77 3.55	6.83 3.57	2.89 3.59	-1.05 3.60	-4.83 3.57	-7.48 3.37	30.4
29.4	47.53 2.46	44.77 2.68	41.03 2.79	37.04 2.84	33.13 2.89	29.19 2.92	25.26 2.96	21.32 3.00	17.39 3.03	13.46 3.06	9.52 3.09	5.58 3.12	1.64 3.14	-2.29 3.15	-5.75 3.04	-8.10 2.79	29.4
28.4	48.17 1.87	45.83 2.23	42.17 2.34	38.41 2.34	34.49 2.41	30.54 2.45	26.60 2.48	22.67 2.52	18.73 2.55	14.80 2.58	10.86 2.62	6.92 2.65	2.97 2.67	-.98 2.70	-4.77 2.68	-7.42 2.47	28.4
27.4	47.64 1.60	44.83 1.82	41.14 1.91	37.14 1.94	33.24 1.97	29.30 2.00	25.36 2.03	21.42 2.06	17.49 2.09	13.56 2.13	9.62 2.16	5.68 2.20	1.73 2.23	-2.21 2.27	-5.68 2.16	-8.03 1.88	27.4
26.4	48.23 .98	45.94 1.36	42.44 1.45	38.50 1.47	34.56 1.49	30.62 1.51	26.68 1.54	22.75 1.57	18.82 1.61	14.89 1.64	10.95 1.68	7.01 1.72	3.06 1.77	-.89 1.81	-4.68 1.81	-7.35 1.58	26.4
25.4	47.67 .73	44.91 .95	41.17 1.03	37.23 1.03	33.29 1.04	29.35 1.06	25.43 1.08	21.50 1.11	17.58 1.15	13.65 1.19	9.72 1.23	5.78 1.28	1.84 1.33	-2.10 1.38	-5.58 1.27	-7.94 .98	25.4
24.4	48.22 .08	45.93 .47	42.43 .55	38.51 .55	34.59 .55	30.65 .55	26.73 .58	22.81 .61	18.89 .65	14.97 .69	11.04 .74	7.11 .80	3.17 .86	-.78 .92	-4.57 .94	-8.00 -.24	24.4
23.3	48.27 -1.28	46.09 -1.65	42.54 -1.76	38.62 -1.79	34.70 -1.79	30.79 -1.78	26.88 -1.76	22.97 -1.73	19.06 -1.69	15.15 -1.65	11.23 -1.59	7.30 -1.53	3.37 -1.46	-.58 -1.38	-4.41 -1.22	-7.12 -.81	23.3
22.3	47.52 -1.77	44.66 -2.13	40.94 -2.25	37.01 -2.28	33.11 -2.30	29.21 -2.30	25.31 -2.28	21.41 -2.26	17.52 -2.22	13.61 -2.16	9.70 -2.10	5.79 -2.03	1.88 -1.95	-2.06 -1.86	-5.51 -1.63	-7.84 -1.14	22.3
21.3	48.12 -2.25	45.97 -2.60	42.44 -2.72	38.55 -2.76	34.65 -2.78	30.77 -2.78	26.89 -2.78	23.01 -2.75	19.13 -2.71	15.24 -2.65	11.34 -2.58	7.43 -2.50	3.51 -2.40	-.42 -2.30	-4.23 -2.11	-6.93 -1.70	21.3
20.3	47.32 -2.73	44.49 -3.10	40.80 -3.24	36.92 -3.29	33.04 -3.32	29.17 -3.33	25.30 -3.33	21.44 -3.30	17.57 -3.26	13.70 -3.19	9.82 -3.11	5.93 -3.01	2.02 -2.90	-1.89 -2.74	-5.31 -2.53	-7.62 -2.06	20.3
19.3	47.49 -3.26	45.77 -3.60	42.28 -3.75	38.42 -3.81	34.56 -3.85	30.71 -3.87	26.87 -3.87	23.03 -3.86	19.18 -3.79	15.33 -3.72	11.47 -3.63	7.60 -3.52	3.71 -3.39	-.20 -3.24	-4.00 -3.02	-6.69 -2.60	19.3
18.3	47.04 -3.75	44.24 -4.12	40.59 -4.29	36.74 -4.37	32.90 -4.42	29.04 -4.45	25.20 -4.45	21.44 -4.43	17.62 -4.37	13.80 -4.29	9.96 -4.19	6.11 -4.06	2.24 -3.91	-1.65 -3.75	-5.05 -3.47	-7.34 -2.98	18.3
17.3	47.57 -4.34	45.49 -4.67	42.03 -4.85	38.22 -4.94	34.41 -5.00	30.61 -5.04	26.82 -5.05	23.04 -5.02	19.25 -4.97	15.44 -4.88	11.65 -4.75	7.82 -4.61	3.97 -4.43	.09 -4.24	-3.68 -3.96	-6.35 -3.51	17.3
16.3	46.66 -4.83	43.89 -5.22	40.28 -5.42	36.44 -5.54	32.70 -5.63	28.93 -5.68	25.18 -5.69	21.43 -5.67	17.68 -5.60	13.92 -5.50	10.14 -5.36	6.35 -5.19	2.53 -4.99	-1.32 -4.77	-4.69 -4.44	-6.96 -3.92	16.3
15.3	47.14 -5.48	45.04 -5.82	41.44 -5.94	37.52 -6.17	34.14 -6.28	30.45 -6.34	26.76 -6.37	23.03 -6.34	19.33 -6.27	15.61 -6.15	11.88 -6.00	8.12 -5.80	4.32 -5.56	.50 -5.30	-3.24 -4.95	-5.89 -4.44	15.3
14.3	46.14 -5.96	43.40 -6.40	39.84 -6.56	36.10 -6.71	32.40 -6.76	28.72 -7.05	25.05 -7.08	21.40 -7.06	17.74 -6.99	14.04 -6.85	10.39 -6.68	6.67 -6.45	2.92 -6.17	-.86 -5.87	-4.19 -5.47	-6.43 -4.88	14.3
13.3	46.56 -6.67	44.55 -7.04	41.14 -7.34	37.50 -7.54	33.94 -7.71	30.21 -7.91	26.51 -7.95	23.01 -7.95	19.42 -7.77	15.81 -7.62	12.18 -7.42	8.52 -7.15	4.82 -6.83	1.06 -6.46	-2.62 -6.00	-5.24 -5.40	13.3
12.2	45.43 -7.15	42.72 -7.67	39.21 -7.82	35.59 -7.99	31.96 -8.09	28.39 -8.32	24.86 -8.39	21.33 -8.39	17.91 -8.30	14.27 -8.14	10.71 -8.20	7.12 -7.89	3.48 -7.52	-.22 -7.09	-3.47 -6.57	-5.67 -5.88	12.2
11.2	45.74 -7.48	43.77 -8.16	40.47 -8.38	36.83 -9.10	33.16 -9.35	29.47 -9.53	25.81 -9.61	22.17 -9.61	18.53 -9.52	14.84 -9.36	12.60 -9.09	9.04 -8.73	5.52 -8.29	1.88 -7.77	-1.73 -7.15	-4.31 -6.40	11.2
10.2	44.40 -8.37	41.74 -9.04	38.29 -9.55	34.77 -9.96	31.13 -10.27	27.71 -10.44	24.56 -10.59	21.21 -10.60	17.47 -10.51	14.52 -10.31	11.14 -10.02	7.73 -9.61	4.25 -9.11	.71 -8.51	-2.43 -7.81	-4.56 -6.92	10.2
9.2	44.53 -9.09	42.60 -9.80	39.43 -10.45	35.81 -10.96	32.67 -11.31	29.34 -11.57	25.12 -11.70	22.88 -11.72	19.65 -11.63	16.41 -11.42	13.15 -11.09	9.85 -10.64	6.50 -10.06	3.06 -9.35	-.39 -8.48	-2.91 -7.46	9.2
8.2	42.78 -9.57	40.21 -10.54	36.93 -11.47	33.44 -11.99	30.44 -12.43	27.25 -12.72	24.14 -12.88	21.02 -12.91	17.90 -12.81	14.80 -12.59	11.65 -12.24	8.51 -11.76	5.31 -11.11	2.04 -10.28	-.85 -9.26	-2.84 -8.01	8.2
7.2	42.47 -10.08	40.59 -11.19	37.75 -12.18	34.49 -12.87	31.65 -13.36	28.64 -13.68	25.64 -13.85	22.65 -13.83	19.66 -13.80	16.68 -13.58	13.70 -13.22	10.71 -12.71	7.71 -12.01	4.66 -11.08	1.61 -9.84	-.70 -8.39	7.2
6.2	40.47 -9.73	38.22 -10.99	35.45 -12.07	32.42 -12.92	29.78 -13.32	26.92 -13.65	24.07 -13.83	21.20 -13.88	18.35 -13.80	15.50 -13.57	12.66 -13.23	9.85 -12.72	7.06 -12.07	4.29 -11.09	1.85 -9.85	.03 -8.38	6.2
	100.0	101.0	102.0	103.0	104.1	105.1	106.1	107.1	108.1	109.1	110.1	111.1	112.2	113.2	114.2	115.2	

R(cm)

TABLE II

COIL ALPHA AT 3500.00 A/(CM*CM) COIL BETA AT 3500.00 A/(CM*CM)

AZ (KGAUSS)
BR (KGAUSS) COIL BETA

Z(cm)	100.0	101.0	102.0	103.0	104.1	105.1	106.1	107.1	108.1	109.1	110.1	111.1	112.2	113.2	114.2	115.2	Z(cm)
68.4	31.00	28.89	26.86	24.74	22.61	20.46	18.31	16.15	13.98	11.80	9.62	7.44	5.25	3.06	1.14	-.23	68.4
	27.29	30.30	31.43	32.57	33.21	33.62	33.83	33.86	33.72	33.40	32.90	32.20	31.29	30.08	28.57	26.88	
67.4	32.58	31.34	29.17	26.75	24.38	22.03	19.69	17.35	15.00	12.65	10.28	7.88	5.43	2.92	.46	-1.28	67.4
	28.32	29.70	30.91	31.82	32.45	32.86	33.08	33.11	32.98	32.67	32.18	31.50	30.61	29.45	27.98	26.34	
66.4	33.61	31.72	29.12	26.45	23.85	21.31	18.79	16.29	13.78	11.26	8.71	6.12	3.47	.72	-1.68	-3.24	66.4
	27.32	28.41	29.39	30.17	30.74	31.12	31.31	31.35	31.21	30.92	30.46	29.82	29.00	27.97	26.75	25.43	
65.4	35.58	34.16	31.61	28.76	25.99	23.28	20.60	17.93	15.26	12.58	9.87	7.10	4.26	1.32	-1.61	-3.62	65.4
	26.10	26.95	27.75	28.41	28.90	29.24	29.41	29.44	29.32	29.04	28.62	28.04	27.31	26.42	25.42	24.37	
64.4	36.05	34.01	31.13	28.14	25.22	22.37	19.54	16.73	13.92	11.10	8.24	5.33	2.34	-.73	-3.42	-5.15	64.4
	24.97	25.58	26.21	26.76	27.18	27.47	27.62	27.64	27.53	27.29	26.90	26.38	25.74	24.97	24.16	23.36	
63.4	37.65	36.12	33.36	30.27	27.24	24.26	21.31	18.37	15.43	12.48	9.49	6.45	3.35	.15	-2.98	-5.12	63.4
	23.82	24.31	24.82	25.29	25.64	25.89	26.02	26.03	25.92	25.69	25.36	24.90	24.35	23.70	23.00	22.35	
62.4	37.82	35.67	32.63	29.44	26.31	23.23	20.17	17.12	14.07	11.01	7.91	4.77	1.56	-1.71	-4.55	-6.37	62.4
	22.73	23.07	23.48	23.85	24.15	24.36	24.47	24.47	24.38	24.19	23.88	23.49	23.00	22.44	21.90	21.43	
61.4	39.19	37.58	34.70	31.45	28.24	25.06	21.91	18.77	15.62	12.46	9.26	6.03	2.74	-.61	-3.88	-6.10	61.4
	21.67	21.91	22.24	22.57	22.82	23.00	23.08	23.09	23.00	22.82	22.56	22.22	21.80	21.32	20.84	20.46	
60.4	39.16	36.92	33.77	30.44	27.17	23.92	20.69	17.46	14.23	10.99	7.72	4.41	1.05	-2.35	-5.30	-7.19	60.4
	20.61	20.75	21.02	21.29	21.51	21.65	21.72	21.72	21.64	21.49	21.26	20.96	20.61	20.19	19.84	19.61	
59.4	40.40	38.72	35.74	32.38	29.04	25.72	22.42	19.12	15.82	12.50	9.16	5.79	2.36	-1.10	-4.46	-6.76	59.4
	19.62	19.69	19.90	20.14	20.32	20.45	20.51	20.50	20.43	20.30	20.10	19.85	19.54	19.18	18.85	18.66	
58.4	40.23	37.91	34.68	31.26	27.87	24.50	21.13	17.77	14.41	11.03	7.63	4.20	.73	-2.76	-5.79	-7.75	58.4
	18.60	18.60	18.77	18.97	19.12	19.23	19.28	19.28	19.22	19.10	18.93	18.71	18.44	18.13	17.93	17.89	
57.4	41.37	39.64	36.59	33.15	29.71	26.29	22.87	19.46	16.04	12.60	9.15	5.67	2.16	-1.39	-4.84	-7.20	57.4
	17.68	17.68	17.74	17.92	18.05	18.15	18.19	18.19	18.14	18.04	17.89	17.70	17.48	17.21	16.99	16.96	
56.4	41.10	38.72	35.41	31.92	28.45	24.98	21.52	18.06	14.60	11.12	7.62	4.10	.55	-3.01	-6.12	-8.12	56.4
	16.87	16.87	16.87	16.92	16.94	17.02	17.07	17.07	17.03	16.94	16.82	16.66	16.46	16.23	16.14	16.26	
55.3	41.50	39.17	35.86	32.33	28.82	25.31	21.81	18.31	14.80	11.28	7.75	4.19	.61	-2.99	-6.12	-8.18	55.3
	16.86	17.30	17.54	17.64	17.79	17.87	17.91	17.91	17.88	17.81	17.70	17.57	17.40	17.21	16.93	16.24	
54.3	42.46	40.61	37.51	33.98	30.44	26.90	23.37	19.83	16.29	12.74	9.17	5.58	1.97	-1.67	-5.18	-7.58	54.3
	15.80	16.32	16.55	16.64	16.78	16.85	16.88	16.89	16.87	16.81	16.73	16.62	16.48	16.31	16.07	15.60	
53.3	42.16	39.80	36.43	32.86	29.29	25.72	22.16	18.60	15.02	11.44	7.84	4.23	.59	-3.06	-6.23	-8.31	53.3
	15.05	15.41	15.61	15.73	15.82	15.89	15.92	15.93	15.92	15.88	15.81	15.72	15.61	15.47	15.18	14.72	
52.3	43.07	41.20	38.05	34.47	30.88	27.29	23.70	20.11	16.51	12.90	9.28	5.64	1.98	-1.70	-5.24	-7.67	52.3
	14.05	14.49	14.68	14.78	14.87	14.93	14.97	14.99	14.98	14.95	14.90	14.83	14.74	14.63	14.46	14.10	
51.3	42.74	40.34	36.94	33.32	29.71	26.10	22.49	18.87	15.25	11.62	7.98	4.32	.65	-3.04	-6.24	-8.35	51.3
	13.12	13.61	13.78	13.88	13.95	14.01	14.05	14.07	14.07	14.05	14.02	13.97	13.90	13.82	13.61	13.27	
50.3	43.62	41.72	38.52	34.90	31.27	27.64	24.01	20.37	16.73	13.09	9.43	5.75	2.06	-1.65	-5.21	-7.67	50.3
	12.37	12.73	12.89	12.98	13.05	13.11	13.15	13.17	13.18	13.17	13.15	13.12	13.07	13.01	12.91	12.66	
49.3	43.25	40.81	37.37	33.73	30.08	26.43	22.79	19.14	15.49	11.82	8.15	4.47	.77	-2.94	-6.16	-8.30	49.3
	11.67	11.99	12.02	12.10	12.17	12.22	12.26	12.29	12.30	12.31	12.30	12.28	12.26	12.22	12.10	11.88	
48.3	44.09	42.16	38.92	35.27	31.61	27.95	24.29	20.63	16.97	13.30	9.61	5.92	2.21	-1.51	-5.09	-7.56	48.3
	10.79	11.05	11.17	11.25	11.31	11.35	11.40	11.43	11.45	11.46	11.46	11.45	11.45	11.45	11.41	11.28	
47.3	43.67	41.19	37.73	34.05	30.39	26.73	23.06	19.39	15.72	12.04	8.35	4.65	.95	-2.77	-5.99	-8.14	47.3
	10.11	10.25	10.33	10.37	10.44	10.49	10.53	10.55	10.59	10.61	10.62	10.63	10.64	10.65	10.62	10.55	
46.3	44.46	42.49	38.24	35.58	31.91	28.24	24.56	20.88	17.20	13.51	9.82	6.13	2.42	-1.29	-4.85	-7.34	46.3
	9.30	9.44	9.50	9.55	9.60	9.65	9.69	9.71	9.74	9.74	9.73	9.72	9.72	9.72	9.74	9.75	
45.3	43.93	41.43	37.99	34.31	30.67	26.99	23.31	19.63	15.94	12.25	8.55	4.86	1.17	-2.50	-5.69	-7.82	45.3
	8.65	8.66	8.65	8.68	8.73	8.73	8.83	8.87	8.91	8.91	8.90	8.88	8.81	8.87	8.15	8.27	
44.3	44.55	42.51	39.31	35.70	32.04	28.37	24.68	20.98	17.29	13.59	9.89	6.20	2.53	-1.12	-4.57	-6.97	44.3
	8.05	8.16	8.18	8.21	8.29	8.35	8.40	8.45	8.49	8.51	8.53	8.55	8.58	8.63	8.78	8.90	
43.3	44.21	41.74	38.36	34.77	31.11	27.43	23.73	20.03	16.32	12.61	8.90	5.21	1.54	-2.07	-5.22	-7.40	43.3
	8.14	8.25	8.27	8.36	8.44	8.52	8.59	8.64	8.68	8.70	8.72	8.72	8.71	8.71	8.67	8.61	
	100.0	101.0	102.0	103.0	104.1	105.1	106.1	107.1	108.1	109.1	110.1	111.1	112.2	113.2	114.2	115.2	

R(cm)

TABLE III

COIL ALPHA AT 1003.30 A/(CM*CM)   COIL BETA AT -1500.00 A/(CM*CM)

BZ (KGAUSS)
BR (KGAUSS)   COIL ALPHA

Z(cm)	100.0	101.1	102.0	103.1	104.1	105.1	106.1	107.1	108.1	109.1	110.1	111.1	112.2	113.2	114.2	115.2	
42.5	14.27	13.74	12.89	11.87	10.89	9.91	8.91	7.92	6.92	5.92	4.91	3.89	2.86	1.80	.74	.00	42.5
	27.09	29.23	31.09	32.51	33.55	34.40	34.73	35.01	35.01	34.75	34.32	33.60	32.59	31.20	29.32	27.19	
41.5	16.44	15.44	14.09	12.61	11.18	10.12	8.88	7.65	6.43	5.19	3.94	2.64	1.30	-.14	-1.41	-2.18	41.5
	26.23	28.25	29.99	31.33	32.33	33.05	33.51	33.75	33.76	33.56	33.09	32.40	31.44	30.16	28.53	26.64	
40.5	19.07	18.34	16.62	15.13	13.55	12.04	10.57	9.12	7.68	6.22	4.73	3.19	1.56	-.20	-2.03	-3.22	40.5
	25.01	26.73	28.19	29.47	30.29	30.95	31.40	31.63	31.64	31.44	31.03	30.40	29.53	28.42	27.06	25.49	
39.5	20.35	19.07	17.17	15.25	13.44	11.71	10.04	8.39	6.74	5.08	3.34	1.62	-.23	-2.21	-3.95	-4.98	39.5
	23.75	25.11	26.34	27.36	28.17	28.74	29.19	29.40	29.42	29.25	28.88	28.33	27.57	26.63	25.49	24.21	
38.5	22.38	21.44	19.58	17.47	15.50	13.59	11.73	9.90	8.07	6.22	4.34	2.39	.35	-1.80	-3.97	-5.36	38.5
	22.40	23.63	24.64	25.59	26.29	26.82	27.19	27.38	27.41	27.26	26.95	26.47	25.83	25.04	24.11	23.06	
37.5	23.17	21.73	19.57	17.36	15.20	13.13	11.11	9.12	7.13	5.12	3.08	.94	-1.20	-3.48	-5.47	-6.65	37.5
	21.25	22.25	23.15	23.91	24.53	25.01	25.35	25.53	25.55	25.43	25.17	24.76	24.22	23.56	22.75	21.86	
36.4	24.41	23.73	21.67	19.34	17.04	14.87	12.72	10.58	8.45	6.30	4.12	1.89	-.42	-2.81	-5.17	-6.67	36.4
	19.99	20.95	21.74	22.40	22.96	23.37	23.66	23.83	23.85	23.77	23.55	23.21	22.76	22.21	21.57	20.81	
35.4	25.40	23.74	21.42	18.93	16.51	14.30	12.02	9.76	7.51	5.24	2.95	.60	-1.80	-4.27	-6.41	-7.69	35.4
	18.94	19.72	20.41	20.98	21.46	21.83	22.10	22.25	22.29	22.22	22.04	21.76	21.39	20.93	20.35	19.67	
34.4	26.58	25.49	23.30	20.73	18.33	15.92	13.54	11.18	8.82	6.45	4.05	1.61	-.88	-3.43	-5.91	-7.50	34.4
	17.75	18.55	19.15	19.66	20.03	20.41	20.65	20.79	20.84	20.79	20.64	20.41	20.11	19.73	19.28	18.69	
33.4	26.96	25.31	22.86	20.24	17.75	15.25	12.79	10.34	7.89	5.43	2.94	.43	-2.13	-4.74	-6.99	-8.35	33.4
	16.40	17.44	17.68	18.42	18.79	19.08	19.30	19.43	19.48	19.44	19.33	19.15	18.89	18.58	18.15	17.61	
32.4	28.16	26.83	24.58	21.95	19.35	16.74	14.24	11.71	9.19	6.65	4.10	1.51	-1.11	-3.74	-6.36	-8.02	32.4
	15.57	16.37	16.85	17.24	17.57	17.83	18.02	18.15	18.20	18.19	18.10	17.95	17.74	17.49	17.17	16.70	
31.4	28.29	26.56	24.02	21.33	18.67	16.05	13.44	10.84	8.25	5.65	3.03	.39	-2.28	-4.99	-7.32	-8.74	31.4
	14.80	15.35	15.76	16.12	16.41	16.65	16.83	16.94	17.00	16.99	16.93	16.82	16.65	16.44	16.11	15.65	
30.4	29.35	27.90	25.61	22.84	20.18	17.50	14.84	12.19	9.54	6.88	4.21	1.52	-1.20	-3.95	-6.60	-8.32	30.4
	13.72	14.34	14.74	15.05	15.30	15.51	15.68	15.79	15.85	15.85	15.81	15.72	15.59	15.43	15.20	14.80	
29.4	29.35	27.56	24.94	22.17	19.43	16.71	14.00	11.30	8.60	5.90	3.18	.45	-2.31	-5.09	-7.49	-8.96	29.4
	12.42	13.40	13.75	14.02	14.25	14.44	14.59	14.70	14.76	14.77	14.75	14.69	14.59	14.46	14.19	13.78	
28.4	30.29	28.84	26.43	23.64	20.86	18.10	15.36	12.62	9.89	7.13	4.38	1.61	-1.19	-4.00	-6.71	-8.47	28.4
	11.47	12.45	12.78	13.02	13.23	13.40	13.53	13.63	13.70	13.72	13.71	13.67	13.59	13.50	13.34	13.00	
27.4	30.20	29.35	25.69	22.95	20.05	17.25	14.43	11.71	8.93	6.16	3.37	.57	-2.25	-5.08	-7.53	-9.05	27.4
	11.13	11.56	11.86	12.07	12.25	12.41	12.53	12.63	12.69	12.73	12.73	12.71	12.66	12.59	12.37	12.00	
26.4	31.05	29.55	27.10	24.25	21.32	18.50	15.73	12.90	10.19	7.39	4.58	1.75	-1.10	-3.96	-6.71	-8.50	26.4
	10.11	10.65	10.93	11.12	11.28	11.42	11.54	11.63	11.70	11.74	11.75	11.75	11.72	11.67	11.57	11.26	
25.4	30.87	28.96	26.28	23.41	20.59	17.72	14.89	12.07	9.25	6.42	3.59	.74	-2.13	-5.00	-7.49	-9.04	25.4
	9.41	9.80	10.05	10.21	10.36	10.49	10.59	10.68	10.75	10.80	10.83	10.84	10.83	10.80	10.63	10.27	
24.4	31.63	30.13	27.51	24.74	21.87	19.02	16.17	13.33	10.49	7.65	4.79	1.93	-.95	-3.85	-6.63	-9.11	24.4
	8.39	8.92	9.15	9.30	9.42	9.54	9.64	9.73	9.79	9.85	9.89	9.91	9.93	9.92	9.87	8.78	
23.3	31.94	30.52	27.94	25.05	22.14	19.31	16.45	13.60	10.75	7.89	5.02	2.15	-.75	-3.66	-6.48	-8.36	23.3
	6.79	6.64	6.70	6.92	6.73	7.04	7.13	7.21	7.28	7.34	7.39	7.43	7.46	7.48	7.56	7.84	
22.3	31.58	29.53	26.78	23.89	21.00	18.12	15.26	12.39	9.53	6.67	3.79	.91	-2.00	-4.90	-7.42	-8.97	22.3
	5.74	5.78	5.82	5.92	6.01	6.11	6.17	6.27	6.35	6.42	6.48	6.53	6.58	6.62	6.77	7.12	
21.3	32.28	30.86	28.27	25.33	22.49	19.62	16.75	13.89	11.02	8.15	5.27	2.38	-.53	-3.45	-6.29	-8.18	21.3
	5.11	4.95	4.97	5.05	5.14	5.22	5.30	5.38	5.45	5.53	5.60	5.67	5.73	5.80	5.92	6.22	
20.3	31.41	29.83	27.06	24.15	21.27	18.39	15.52	12.66	9.79	6.92	4.04	1.15	-1.76	-4.68	-7.20	-8.76	20.3
	4.29	4.10	4.10	4.17	4.24	4.31	4.38	4.46	4.54	4.62	4.70	4.79	4.87	4.95	5.13	5.50	
19.3	32.49	31.08	28.50	25.61	22.73	19.86	16.99	14.13	11.27	8.41	5.53	2.66	-.27	-3.20	-6.06	-7.93	19.3
	3.43	3.25	3.25	3.30	3.35	3.41	3.48	3.56	3.64	3.71	3.82	3.92	4.03	4.13	4.30	4.63	
18.3	31.35	29.94	27.21	24.32	21.45	18.59	15.73	12.88	10.03	7.13	4.31	1.42	-1.48	-4.39	-6.90	-8.47	18.3
	2.52	2.41	2.38	2.41	2.44	2.49	2.55	2.63	2.71	2.81	2.92	3.04	3.16	3.29	3.51	3.90	
17.3	32.58	31.13	28.61	25.71	22.87	20.02	17.19	14.35	11.52	8.68	5.82	2.95	.06	-2.86	-5.69	-7.59	17.3
	1.73	1.55	1.50	1.52	1.54	1.58	1.63	1.70	1.79	1.90	2.02	2.16	2.31	2.47	2.69	3.06	
16.3	31.96	29.96	27.25	24.34	21.58	18.73	15.94	13.07	10.26	7.44	4.51	1.75	-1.13	-4.03	-6.52	-8.08	16.3
	.93	.70	.62	.60	.61	.63	.68	.75	.86	.95	1.10	1.25	1.43	1.62	1.89	2.32	
15.3	32.52	31.14	28.59	25.73	22.92	20.12	17.33	14.54	11.76	8.95	6.15	3.32	.46	-2.43	-5.25	-7.13	15.3
	.00	-.14	-.29	-.32	-.34	-.33	-.29	-.21	-.13	-.00	.15	.34	.55	.77	1.07	1.49	
14.3	31.41	29.83	27.14	24.31	21.51	18.76	15.98	13.23	10.48	7.72	4.94	2.14	-.59	-3.55	-6.02	-7.56	14.3
	-.78	-1.06	-1.19	-1.25	-1.31	-1.32	-1.29	-1.23	-1.13	-.99	-.81	-.59	-.36	-.10	.24	.73	
13.3	32.30	30.94	28.42	25.52	22.75	20.12	17.40	14.70	11.99	9.24	6.55	3.78	.99	-1.86	-4.64	-6.52	13.3
	-1.76	-1.97	-2.14	-2.25	-2.31	-2.35	-2.34	-2.29	-2.19	-2.03	-1.83	-1.58	-1.30	-.94	-.59	-.09	
12.2	31.47	29.50	26.64	24.07	21.35	18.65	15.99	13.33	10.68	8.02	5.34	2.63	-.12	-2.92	-5.34	-6.86	12.2
	-2.50	-2.85	-3.08	-3.24	-3.35	-3.41	-3.41	-3.37	-3.26	-3.09	-2.87	-2.59	-2.26	-1.89	-1.45	-.86	
11.2	31.56	30.51	28.04	25.31	22.64	20.01	17.40	14.81	12.22	9.63	7.01	4.37	1.57	-1.08	-3.81	-5.66	11.2
	-3.48	-3.80	-4.09	-4.27	-4.45	-4.54	-4.57	-4.53	-4.42	-4.24	-3.99	-3.67	-3.29	-2.84	-2.31	-1.67	
10.2	30.83	28.83	26.27	23.60	20.99	18.42	15.89	13.37	10.85	8.35	5.81	3.24	.53	-2.05	-4.38	-5.85	10.2
	-4.23	-4.71	-5.09	-5.37	-5.59	-5.71	-5.76	-5.73	-5.62	-5.43	-5.15	-4.77	-4.35	-3.83	-3.23	-2.47	
9.2	31.05	29.72	27.34	24.75	22.22	19.75	17.30	14.87	12.45	10.02	7.58	5.11	2.59	-.00	-2.61	-4.41	9.2
	-5.18	-5.71	-6.19	-6.55	-6.82	-6.99	-7.06	-7.04	-6.93	-6.73	-6.43	-6.03	-5.52	-4.91	-4.16	-3.29	
8.2	29.55	27.77	25.29	22.83	20.38	18.01	15.66	13.33	11.00	8.69	6.35	4.00	1.60	-.85	-2.98	-4.33	8.2
	-5.91	-6.70	-7.32	-7.79	-8.11	-8.32	-8.41	-8.41	-8.29	-8.08	-7.76	-7.34	-6.77	-6.05	-5.18	-4.11	
7.2	29.59	28.17	26.08	23.77	21.44	19.24	17.01	14.78	12.56	10.35	8.13	5.92	3.69	1.42	-.84	-2.48	7.2
	-6.66	-7.54	-8.32	-8.85	-9.24	-9.47	-9.59	-9.59	-9.49	-9.27	-8.95	-8.50	-7.89	-7.09	-6.02	-4.78	
6.2	27.47	26.24	24.18	22.05	19.85	17.42	15.71	13.54	11.47	9.37	7.27	5.21	3.16	1.11	-.62	-1.83	6.2
	-6.66	-7.64	-8.55	-9.13	-9.52	-9.77	-9.89	-9.91	-9.82	-9.60	-9.29	-8.85	-8.24	-7.44	-6.37	-5.11	

100.0 101.0 102.0 103.0 104.1 105.1 106.1 107.1 108.1 109.1 110.1 111.1 112.2 113.2 114.2 115.2

R(cm)

TABLE IV

COIL ALPHA AT 3000.00 A/(CM*CM) COIL BETA AT -1500.00 A/(CM*CM)

BZ (KGAUSS)
BR (KGAUSS) COIL BETA

Z (cm)	100.0	101.0	102.0	103.0	104.1	105.1	106.1	107.1	108.1	109.1	110.1	111.1	112.2	113.2	114.2	115.2	Z (cm)
68.4	.84	.90	1.32	1.74	2.22	2.66	3.10	3.54	3.97	4.40	4.83	5.27	5.70	6.14	6.46	6.56	68.4
	3.28	1.95	1.35	.91	.58	.35	.19	.11	.09	.14	.26	.46	.74	1.15	1.67	2.28	
67.4	-.11	-.02	.45	1.02	1.56	2.08	2.59	3.09	3.59	4.08	4.59	5.11	5.64	6.21	6.76	7.00	67.4
	3.25	2.65	2.11	1.69	1.38	1.15	1.00	.92	.91	.95	1.07	1.26	1.53	1.91	2.42	3.00	
66.4	-.39	-.04	.61	1.27	1.89	2.49	3.06	3.62	4.17	4.73	5.30	5.89	6.50	7.16	7.68	7.84	66.4
	4.12	3.65	3.22	2.87	2.60	2.40	2.26	2.19	2.17	2.21	2.32	2.49	2.73	3.06	3.45	3.89	
65.4	-1.06	-.92	-.31	.42	1.10	1.75	2.38	3.00	3.61	4.23	4.85	5.50	6.19	6.92	7.65	8.00	65.4
	5.09	4.74	4.40	4.11	3.88	3.71	3.59	3.52	3.50	3.54	3.63	3.78	3.98	4.23	4.53	4.84	
64.4	-1.07	-.68	.06	.84	1.57	2.27	2.94	3.60	4.26	4.93	5.60	6.30	7.04	7.81	8.43	8.64	64.4
	6.04	5.80	5.55	5.32	5.14	4.98	4.88	4.82	4.81	4.83	4.90	5.02	5.18	5.38	5.59	5.79	
63.4	-1.54	-1.38	-.71	.09	.86	1.59	2.31	3.01	3.70	4.40	5.12	5.86	6.63	7.44	8.24	8.62	63.4
	7.00	6.84	6.65	6.46	6.31	6.19	6.11	6.06	6.05	6.08	6.12	6.20	6.32	6.47	6.62	6.74	
62.4	-1.39	-.97	-.19	.63	1.42	2.19	2.93	3.66	4.38	5.11	5.85	6.62	7.42	8.25	8.91	9.14	62.4
	7.96	7.87	7.79	7.61	7.49	7.40	7.33	7.29	7.27	7.28	7.32	7.37	7.46	7.56	7.64	7.67	
61.4	-1.72	-1.56	-.86	-.02	.78	1.57	2.33	3.07	3.82	4.57	5.33	6.12	6.93	7.78	8.61	9.00	61.4
	8.92	8.89	8.80	8.71	8.62	8.56	8.50	8.47	8.46	8.45	8.47	8.50	8.55	8.60	8.65	8.63	
60.4	-1.44	-1.02	-.22	.61	1.44	2.24	3.01	3.77	4.52	5.24	6.06	6.85	7.68	8.53	9.20	9.43	60.4
	9.88	9.91	9.88	9.82	9.77	9.72	9.69	9.66	9.64	9.63	9.63	9.64	9.65	9.67	9.65	9.56	
59.4	-1.67	-1.50	-.80	.05	.87	1.66	2.44	3.20	3.96	4.72	5.50	6.30	7.12	7.96	8.81	9.20	59.4
	10.84	10.92	10.92	10.90	10.88	10.86	10.84	10.82	10.80	10.78	10.76	10.75	10.73	10.71	10.66	10.53	
58.4	-1.27	-.85	-.05	.80	1.61	2.40	3.17	3.93	4.69	5.45	6.22	7.01	7.83	8.69	9.35	9.57	58.4
	11.81	11.95	12.00	12.01	12.02	12.02	12.01	12.00	11.98	11.96	11.92	11.88	11.84	11.78	11.68	11.46	
57.4	-1.41	-1.25	-.55	.24	1.09	1.87	2.63	3.38	4.12	4.87	5.63	6.41	7.22	8.06	8.88	9.26	57.4
	12.76	12.96	13.05	13.10	13.13	13.16	13.17	13.16	13.14	13.11	13.08	13.00	12.92	12.83	12.69	12.46	
56.4	-.49	-.47	.31	1.14	1.93	2.69	3.43	4.16	4.88	5.61	6.35	7.11	7.90	8.72	9.36	9.57	56.4
	13.75	14.00	14.14	14.23	14.30	14.35	14.37	14.38	14.36	14.32	14.25	14.16	14.05	13.92	13.71	13.39	
55.3	-.62	-.24	.62	1.33	2.10	2.84	3.55	4.25	4.94	5.63	6.35	7.08	7.85	8.64	9.27	9.47	55.3
	14.25	14.31	14.42	14.55	14.66	14.73	14.78	14.79	14.77	14.72	14.63	14.52	14.38	14.21	14.09	14.04	
54.3	-.54	-.39	.25	1.01	1.77	2.47	3.14	3.80	4.45	5.11	5.79	6.49	7.22	7.99	8.75	9.07	54.3
	15.30	15.37	15.44	15.51	15.58	15.65	15.68	15.65	15.64	15.57	15.47	15.32	15.54	15.34	15.12	14.98	
53.3	.15	.50	1.21	1.95	2.66	3.32	3.95	4.56	5.16	5.77	6.39	7.05	7.74	8.47	9.05	9.20	53.3
	16.24	16.43	16.67	16.89	17.08	17.22	17.31	17.35	17.33	17.26	17.13	16.95	16.73	16.47	16.24	16.05	
52.3	.39	.69	1.08	1.79	2.63	3.04	3.61	4.15	4.69	5.24	5.81	6.41	7.05	7.74	8.43	8.70	52.3
	17.30	17.53	17.66	18.12	18.36	18.54	18.65	18.70	18.69	18.63	18.45	18.24	17.97	17.66	17.33	17.04	
51.3	1.24	1.54	2.19	2.84	3.44	3.97	4.47	4.95	5.41	5.88	6.37	6.90	7.49	8.12	8.62	8.72	51.3
	18.27	18.65	19.04	19.39	19.58	19.91	20.00	20.12	20.11	20.01	19.84	19.59	19.26	18.88	18.50	18.14	
50.3	1.68	1.73	2.22	2.42	3.19	3.74	4.20	4.59	4.96	5.34	5.75	6.20	6.70	7.28	7.88	8.08	50.3
	19.36	19.81	20.29	20.73	21.09	21.36	21.54	21.63	21.61	21.50	21.29	20.99	20.61	20.16	19.66	19.18	
49.3	2.77	3.00	3.53	4.05	4.58	4.84	5.15	5.42	5.69	5.98	6.26	6.61	7.03	7.52	7.90	7.93	49.3
	20.48	21.01	21.61	22.14	22.58	22.91	23.13	23.23	23.21	23.08	22.84	22.49	22.03	21.49	20.92	20.33	
48.3	3.48	3.44	3.40	4.21	4.85	4.79	4.97	5.12	5.25	5.40	5.57	5.80	6.11	6.51	6.97	7.09	48.3
	21.51	22.26	22.99	23.64	24.19	24.56	24.82	24.95	24.93	24.74	24.50	24.08	23.55	22.90	22.18	21.44	
47.3	4.30	5.02	5.38	5.64	5.88	5.97	6.01	6.01	5.99	5.93	6.02	6.10	6.27	6.55	6.75	6.68	47.3
	22.61	23.58	24.48	25.29	25.98	26.35	26.55	26.61	26.59	26.52	26.30	25.91	25.18	24.41	23.56	22.64	
46.3	6.00	5.92	5.97	6.12	6.19	6.07	5.93	5.76	5.57	5.40	5.25	5.17	5.17	5.30	5.53	5.52	46.3
	23.41	24.90	26.08	27.00	27.76	28.24	28.64	28.82	28.81	28.61	28.24	27.69	26.95	26.04	24.97	23.83	
45.3	7.92	7.87	7.92	7.97	7.83	7.41	7.09	6.71	6.33	5.96	5.62	5.33	5.12	5.04	4.95	4.68	45.3
	25.00	26.50	27.94	29.34	29.74	30.42	30.82	31.02	31.01	30.80	30.38	29.76	28.91	27.84	26.55	25.10	
44.3	9.70	9.28	9.00	8.87	8.24	7.72	7.10	6.58	5.99	5.41	4.84	4.31	3.84	3.49	3.25	2.97	44.3
	26.21	27.04	29.66	30.94	31.04	32.54	33.02	33.24	33.24	33.01	32.56	31.88	30.93	29.69	28.11	26.30	
43.3	12.22	11.78	11.14	10.51	9.79	8.98	8.20	7.49	6.87	6.26	4.95	4.15	3.37	2.64	1.96	1.39	43.3
	28.90	29.09	30.90	32.38	33.61	34.14	34.51	34.84	34.94	34.81	34.14	33.92	32.61	31.06	29.30	27.23	

100.0 101.0 102.0 103.0 104.1 105.1 106.1 107.1 108.1 109.1 110.1 111.1 112.2 113.2 114.2 115.2

R(cm)

A coarse map of the absolute value of the field B is shown in Figs. 7 and 8 for the $J_\alpha = J_\beta = 3500$ A/cm^2 and $J_\alpha = 3000$, $J_\beta = -1500$ A/cm^2 respectively. In these figures the field values, always expressed in Kgauss, are written on the corresponding points of the entire POISCR region. Just outside the yoke, i. e. $z = 150$ cm and $r = 210$ cm, only the average value of B is given, since POISCR calculations exhibit large fluctuations on the calculated values. These fluctuations are due to the local irregular zoning and to the boundary between iron and air.

3. - ATTRACTIVE FORCES BETWEEN THE COILS.

In an ideal situation, i. e. when the median plane and the axis of the magnet and the coils coincide, the only forces acting on the coils are an axial force, F_z, induced by the radial component of the field (F_z being equal in magnitude and opposite in sign for the coils above and below the median plane) and a radial and a tangential stresses induced by the axial component of the field. Evaluations of the radial and tangential stresses are reported elsewhere[2, 6].

The axial forces are then simply given by $F_z = 2\pi J \int B_r(r, z)\, r\, dr\, dz$ where the integral is extended over the coil region, J is the average current density inside the coils and B_r is the radial field component calculated with the POISCR code. The forces thus obtained for the coil α, F_z^α, the coil β, F_z^β, and their sum, F_z^{tot}, are listed in Table V for the two

TABLE V - Attractive forces between the coils.

J_α (A/cm^2)	J_β (A/cm^2)	$\bar{B}$ (R = 40 cm) (Kgauss)	F_z^α (Tons)	F_z^β (Tons)	F_z^{tot} (Tons)
3500	3500	50.68	+ 91	- 1667	- 1576
3000	- 1500	31.51	- 1114	+ 593	- 521

limiting cases. The forces are expressed in Tons, the negative sign meaning actractive forces between the coils above and below the median plane. The magnetic field on the median plane at $r = 40$ cm is listed as an indication of the field level. In the case $J_\alpha = J_\beta = 3500$ A/cm^2 the coil α is attracted toward the median plane with a force of 1667 Tons while the coil β is pushed away with a force of 91 Tons, the resultant being obviously toward the midplane. In the other case, instead, the upper coil is pushed away by 593 Tons while the lower one is attracted toward the median plane by 1114 Tons, the resultant being 521 Tons toward the median plane.

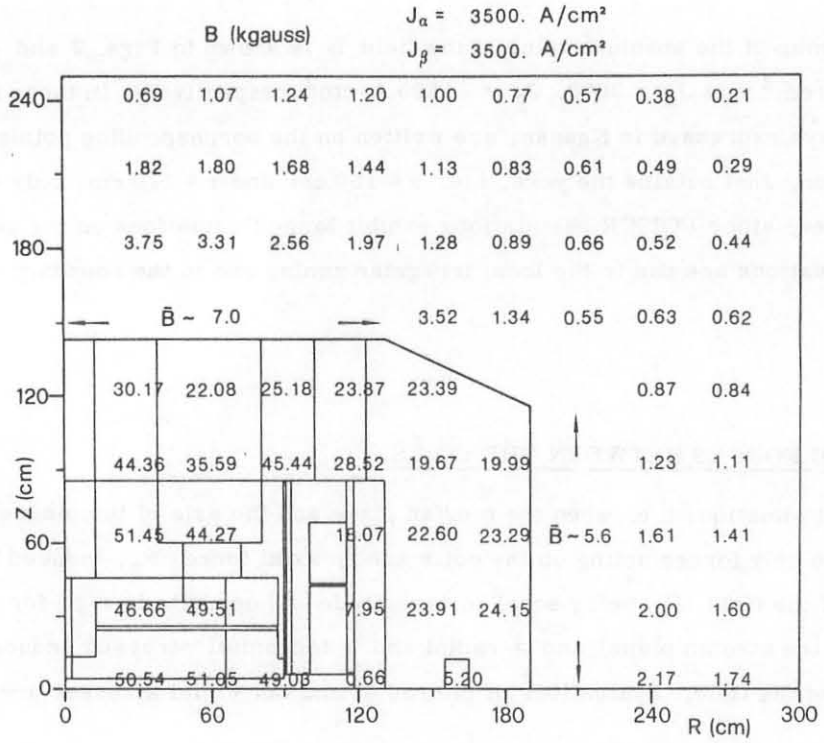

FIG. 7 - Calculated absolute values of the field B at different points over the entire POISCR area for the case $J_\alpha = J_\beta = 3500\ A/cm^2$.

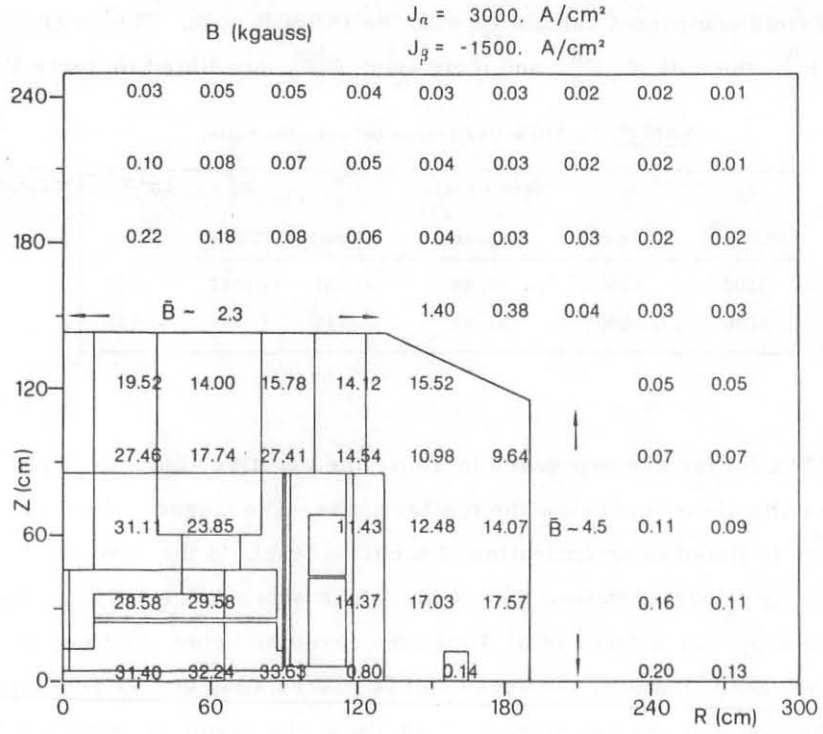

FIG. 8 - Calculated absolute values of the field B at different points over the entire POISCR area for the case $J_\alpha = 3000$, $J_\beta = 1500\ A/cm^2$.

Lines of constant axial forces are plotted with steps of 0.5 Tons in Fig. 9, on the left for the $J_\alpha = J_\beta = 3500\ A/cm^2$ case and on the right for the $J_\alpha = 3000\ A/cm^2$, $J_\beta = -1500\ A/cm^2$.

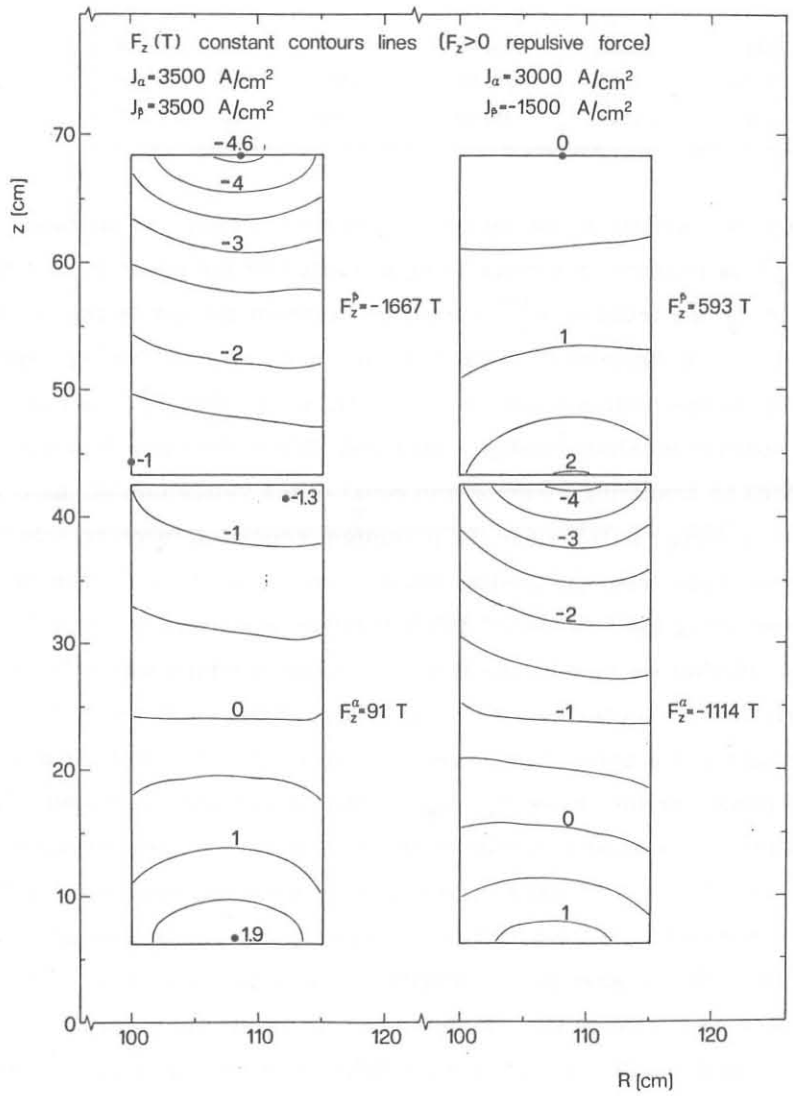

FIG. 9 - Lines of constant axial force on the coils drawn at intervals of 0.5 Tons. On the right of the figure the $J_\alpha = J_\beta = 3500\ A/cm^2$ case, on the left the $J_\alpha = 3000$, $J_\beta = -1500\ A/cm^2$ case.

The magnitude of the repulsive force on the coil β has been calculated also for $J_\beta = -1500\ A/cm^2$ with $J_\alpha = 2000$ and $3000\ A/cm^2$ and $J_\beta = -2500$, $J_\alpha = 3000\ A/cm^2$, even though the latter case is well outside the operating diagram of the machine. The expected forces are of comparable magnitude for the two $J_\beta = -1500\ A/cm^2$ cases, while they almost double in going to $J_\beta = -2500\ A/cm^2$. Their values are reported in Table VI.

TABLE VI - Attractive forces between the coils ($J_\beta < o$).

J_α (A/cm^2)	J_β (A/cm^2)	$\bar{B}$ (R = 40 cm) (Kgauss)	F_z^α (Tons)	F_z^β (Tons)	F_z^{tot} (Tons)
3500	- 1500	35.30	- 1438	+ 690	- 748
3000	- 2500	27.01	- 1509	+ 1140	- 369
2000	- 1500	22.90	- 590	+ 423	- 167

At very low coils excitation, as during the ramping to reach an operating point, the total axial force F_z^{tot} is positive, the coils being attracted by the upper part of the yoke. For the case J_α equal to J_β the trend of F_z^{tot} versus the current density is shown in Fig.10. The solid line, obtained using a "standard" POISCR model, i. e. with hill-valley regions simulated by iron rings with magnetization fraction F = 0.383, shows that F_z^{tot} is repulsive to J $\sim$ $\sim$ 800 A/cm^2, the positive maximum being $\sim$20 Tons. The broken line is a more conservative estimate obtained by assuming a sector gap equal to the valley height, as it is for the coils parts along the valleys. In this case the maximum repulsive force is $\sim$54 Tons and the axial force is directed away from the median plane up to $\sim$1150 A/cm^2. The values of F_z^α, F_z^β and F_z^{tot} obtained using the "standard" POISCR model are listed in Table VII.

Since these calculations rely on the magnetic fields obtained with a POISCR model there are, obviously, uncertainties related to the choice of the mesh and to the truncation errors. The sensitivity of the calculated forces to different POISCR fields can be inferred form Table VIII. Listed, for the cases $J_\alpha = J_\beta = 3500$ A/cm^2 and $J_\alpha = 3000$, $J_\beta = -1500$ A/cm^2, are the values of the axial forces obtained with quite different relaxation grids labeled as GRC2, GR8, DJ. The GRC2 case corresponds to the mesh presented in Fig. 3 and to the final cyclotron geometry, the other two refer to previous calculations with slightly different geometries and with a higher points density in the midplane region. Only a variation of roughly 10% is observed between the maximum and the minimum values of F_z^{tot}. The geometrical differences are quite small for the GRC2 and GR8 cases like a difference of 0.3 mm in the minimum distance from the median plane of the iron part of the inner cryostat wall and the dimensions of the penetrations on the median plane region. Larger geometrical differences are instead present in the DJ case which involves a 2 mm difference in the sectors dimensions, the minimum coils distance from the median plane (6.35 cm in the DJ case against 6.2 cm of the other two cases) and the dimensions of the holes through the upper part of the yoke.

TABLE VII - Forces between the coils at low coils excitation.

J_α (A/cm^2)	J_β (A/cm^2)	$\overline{B}$ (R = 40 cm) (Kgauss)	F_z^α (Tons)	F_z^β (Tons)	F_z^{tot} (Tons)
1750	1750	32.90	+ 89	- 383	- 294
1050	1050	25.13	+ 61	- 111	- 50
700	700	20.75	+ 44	- 36	+ 8
525	525	18.31	+ 34	- 14	+ 20
300	300	14.69	+ 19	+ 2	+ 21

TABLE VIII - Attractive forces between the coils for three different POISCR models.

J_α (A/cm^2)	J_β (A/cm^2)	$\overline{B}$ (R = 40 cm) (Kgauss)	F_z^α (Tons)	F_z^β (Tons)	F_z^{tot} (Tons)	
3500	3500	50.68	+ 91	- 1667	- 1576	GRC2
3000	- 1500	31.51	- 1114	+ 593	- 521	
3500	3500	50.50	+ 105	- 1733	- 1628	G8
3000	- 1500	31.27	- 1110	+ 600	- 510	
3500	3500	50.43	+ 114	- 1571	- 1477	DJ
3000	- 1500	32.19	- 1052	+ 571	- 481	

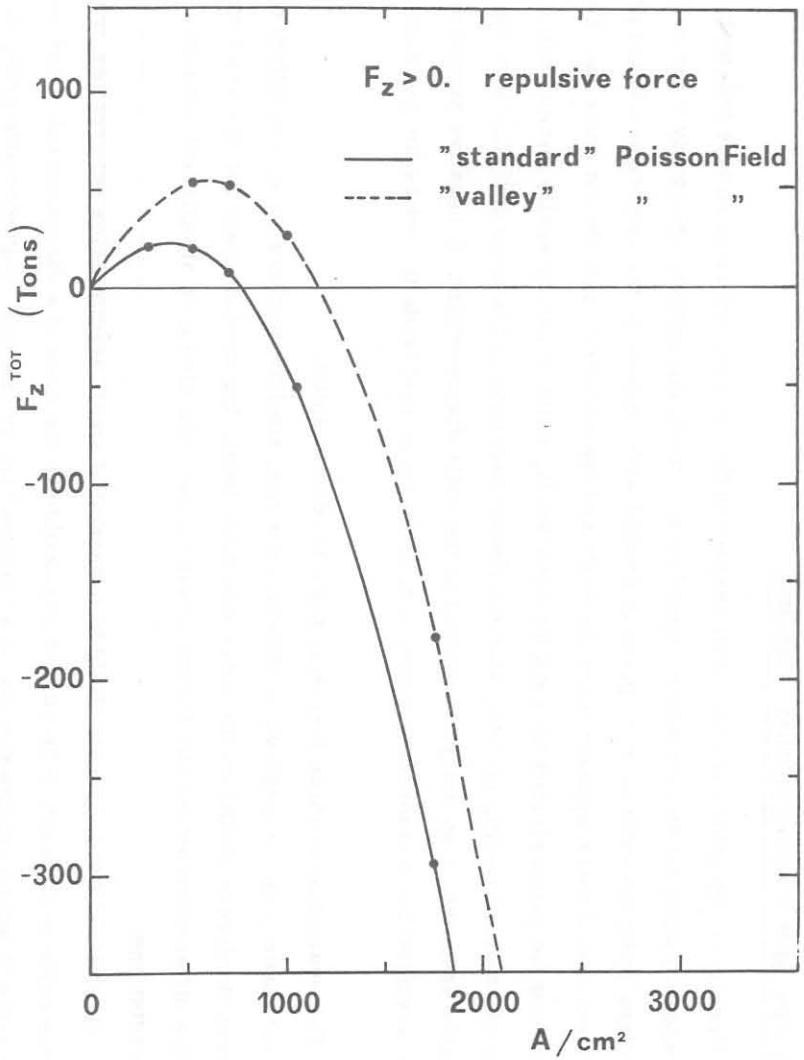

FIG.10 - Axial force F_z^{tot} plotted as a function of the average current density. See text for details.

4. - FORCES DUE TO POSITIONING ERRORS.

Errors in centering the coils with respect to the iron structure introduce magnetic forces whose magnitude and direction depend on the centering errors. Obviously a net axial force arises when the coils median plane is shifted with respect to the cyclotron median plane and a net radial force appears when the coils and the cyclotron axis do not coincide. These forces can be parametrized by a spring constant K, since it can be easily shown that in the case of small centering errors, where a linear variation of the magnetic field can be reasonably assumed, they are proportional to the coils displacement. A negative spring constant is assumed for a stabilizing force, i. e. for a force that tends to reduce the positioning error.

The evaluation of these forces is quite uncertain since:

a) The net force must be obtained as difference among similar numbers, i. e. the difference between the forces acting on the coils above and below the median plane for the axial case and the differences among the forces acting on the coils elements at different azimuths for the radial one.

b) The calculation of the magnetic field in presence of small asymmetries between the iron and the coils is difficult. It is almost impossible in the case of a displacement of the coils axis since it would require the use of a "proved" tridimensional magnetostatic code. It is uncertain also in the case of a median plane shift, although this problem retains full cylindrical symmetry.

Bearing the difficulties of an exact calculation of the field, an estimate of the net forces has been carried out for both types of error using a model, referred below as "iron field model", which involves only magnetic fields symmetric with respect to the midplane and to the cyclotron axis as those obtained with the relaxation grid presented in Fig. 3. Only for the case of an axial shift we tried to use a magnetic field calculated in an asymmetric configuration. The results obtained in this way are referred in the following as "non symmetric field model."

4. 1. - Iron field model.

It has been assumed that: i) The coils have the exact design geometry, including full cylindrical symmetry; ii) The total magnetic field, $B_{Poisson}(r,z)$ can be written as the sum of the field generated by the air-core coils, $B_{Coils}(r,z)$ and the field generated by the iron, $B_{Iron}(r,z)$, the coils component being indipendently computed; iii) The B_{Iron} field is not sensitive to small variations (a few mm) of the coils position.

Under these hypothesis the force can be calculated by integrating the expression $\underline{dF} = i \cdot \underline{dl} \wedge \underline{B}_{Iron}$, over the displaced coils.

The procedure can be affected by large errors mainly due to uncertainties in the B_{Iron} component. The latter is in fact a relatively small quantity obtained as a difference between similar numbers $B_{Poisson}$ and B_{Coils}. As an example the radial component of B_{Iron}, averaged from the inner to the outer coils radii, is plotted as a function of z in Fig. 11 for the

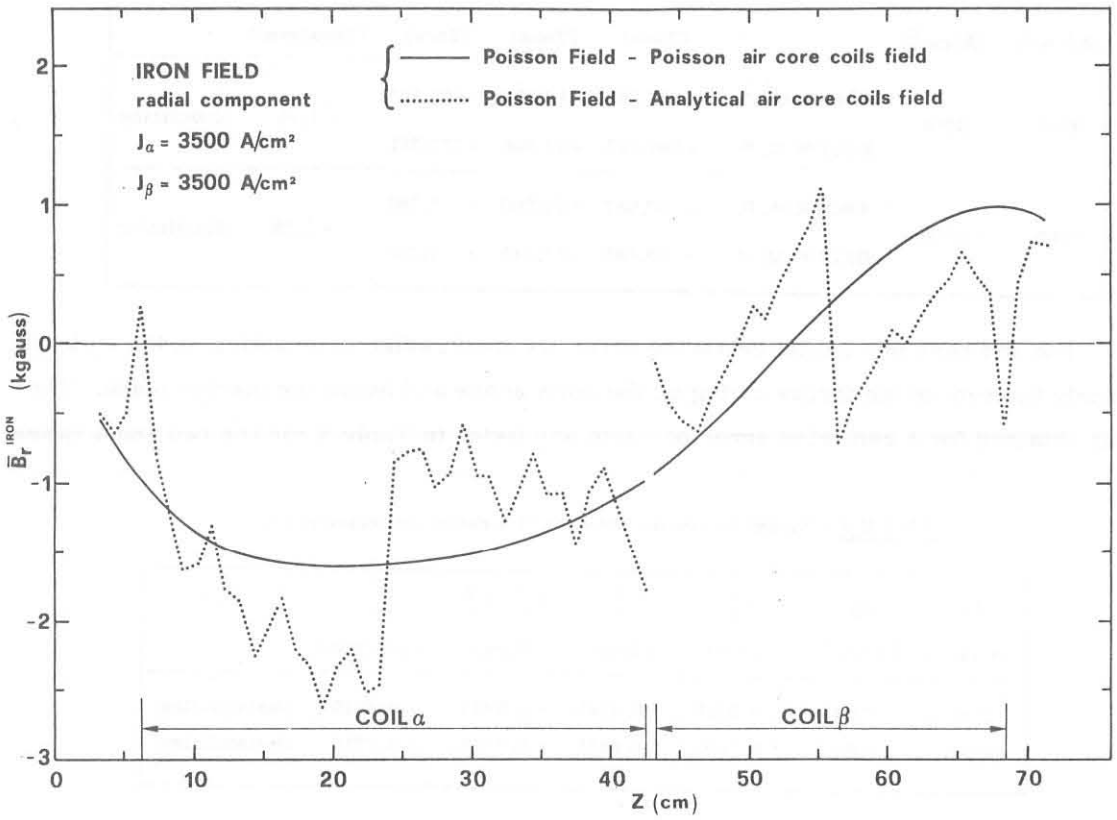

FIG. 11 - Average radial component of the iron field plotted as a function of z for the $J_\alpha = J_\beta = 3500$ A/cm^2

case $J_\alpha = J_\beta = 3500$ A/cm^2. The solid line is the B_{Iron} component obtained by subtracting from the total field the air core coils field calculated with the POISCR program and with the same relaxation grid used for the total field. The broken line has been obtained by subtracting from the total field the exact analytical coils field and it exhibits large, unphysical fluctuations probably due to the truncation errors. Therefore the POISCR code has been used to calculate consistently both the total and the air core coils fields.

The axial forces F_z^α, F_z^β, F_z^{tot} obtained in the case of a median plane error of 1 mm are listed separately for the coils above and below the median plane in Table IX for the two limiting cases $J_\alpha = J_\beta = 3500$ A/cm^2 and $J_\alpha = 3000$, $J_\beta = -1500$ A/cm^2. The net axial force is expressed in terms of the spring constant, i. e. Tons/mm. The magnitude of the for-

ces acting on the coils above and below the median plane indicates that the net force, around 1. 5 Tons/mm, is stabilizing in both cases.

TABLE IX - Axial forces for the case of a media plane error.

J_α (A/cm^2)	J_β (A/cm^2)		F_z^α (Tons)	F_z^β (Tons)	F_z^{tot} (Tons)	K_z (Tons/mm)	
3500	3500	ABOVE M. P.	+ 187.762	- 18.359	+ 169.403	- 1.35	Stabilizing
		BELOW M. P.	- 187.752	+ 17.001	+ 170.751		
3000	- 1500	ABOVE M. P.	- 60.987	+ 54.200	- 6.787	- 1.55	Stabilizing
		BELOW M. P.	+ 59.785	- 54.549	+ 5.236		

For the case of a radial centering error the total radial force acting on the coils is obviously the sum of the forces acting on the coils above and below the median plane. The forces obtained for a centering error of 1 mm are listed in Table X for the two usual cases.

TABLE X - Radial forces for the case of a radial centering error.

J_α (A/cm^2)	J_β (A/cm^2)	F_z^α (Tons)	F_z^β (Tons)	$F_z^\alpha + F_z^\beta$ (Tons)	K_r (Tons/mm)	
3500	3500	- 0. 0026	+ 0. 3390	+ 0. 3365	+ 0. 6729	Destabilizing
3000	- 1500	+ 0. 3003	+ 0. 0875	+ 0. 3878	+ 0. 7756	Destabilizing

The radial forces acting on the coil α, the coil β and their sum are given together with the spring constant. The values obtained are nearly equal, 0. 67 Tons/mm for the $J_\alpha = J_\beta = 3500$ A/cm^2 and 0. 78 Tons/mm for the $J_\alpha = 3000$, $J_\beta = -1500$ A/cm^2, and the forces are in both cases unstabilizing. Calculations done on other cases where J_β is negative have shown that the radial force is $\sim$0. 9 Tons/mm in the $(J_\alpha, J_\beta) = (3500, -1500)$ A/cm^2 case and can reach 1. 9 Tons/mm in the extreme case of $(J_\alpha, J_\beta) = (3000, -2500)$ A/cm^2.

4. 2. - Non symmetric field model.

A relaxation grid covering the regions above and below the median plane can be used to obtain the magnetic field in the case of a median plane error. Sine the main drawback of this procedure is a poorer mesh resolution, these calculations have been carried out only for the case of a rather large mid-plane error, z = 2 cm, namely a distance corresponding to the mesh size of the grid used for this model. Otherwise it is likely that the differences in

the B_r field component above and below the median plane are just due to the different distribution of the relaxation points. In fact the inspection of the field maps has shown that also in the case of a midplane shift of 2 cm the differences in B_r are, on the average, a few hundred of Gauss at maximum, i. e. only a few percents or less of the field value.

The results obtained with this model are presented in Table XI which lists the forces acting an the coils above and below the median plane and the resultant net force. These calculations indicate that the coils are in unstable equilibrium. Assuming that the force is proportional to the median plane error, the axial spring constants are ~ 0.6 Tons/mm for the $J_\alpha = J_\beta = 3500$ A/cm^2 case and ~ 1 Tons/mm for the $J_\alpha = 3000$, $J_\beta = -1500$ A/cm^2 case and so they are roughly comparable in magnitude with the results obtained integrating over the B_{Iron}.

TABLE XI - Axial forces for the case of a median plane error of 2 cm (Non symmetric field model).

J_α (A/cm^2)	J_β (A/cm^2)		F_z^α (Tons)	F_z^β (Tons)	F_z^{tot} (Tons)	Net force (Tons)	K_z (Tons/mm)	
3500	3500	ABOVE M. P.	+ 89.119	- 1680.455	- 1591.335	+ 11.48	+ 0.57	Destabilizing
		BELOW M. P.	- 71.407	+ 1674.222	+ 1602.815			
3000	- 1500	ABOVE M. P.	- 1107.007	+ 591.959	- 515.048	+ 22.89	+ 1.15	Destabilizing
		BELOW M. P.	+ 1131.588	- 593.648	+ 537.940			

5. - CONCLUSIONS.

The calculation of the attractive forces between the coils have given a maximum force of 1576 Tons for the case $J_\alpha = J_\beta = 3500$ A/cm^2 corresponding to an average pressure of 153 Kg/cm^2 exerted by each coil, above and below the median plane, on the central ring of the cryostat. The repulsive forces between the α and β sections of the coils are around 600 Tons for the case $J_\alpha = 3000$, $J_\beta = -1500$ A/cm^2, chosen as the more critical one for the acceleration of ions with $Z/A \leq 0.5$. From a crude interpolation between the results obtained for the cases $J_\alpha = 3000$ A/cm^2 with $J_\beta = -1500$ and -2500 A/cm^2 the repulsive forces at the coils excitations necessary to accelerate the $^3He^{++}$ beams will be less than 850 Tons.

While the evaluation of these attractive forces is relatively accurate, as the close results obtained using different Poisson fields confirm, serious uncertainties remain on the magnitude and direction of the forces introduced by the centering errors. This is quite apparent from the contradictory results on the axial spring constant obtained with the two models used. It should be noted that the two models are really different, since the "non symme

tric field model" uses the total fields obtained assuming a large coils displacement (so changing drastically the iron-coils geometry), while the other one assumes the independence of the iron field from the centering errors. There is no way to say which model is the right one, but it can be said only that the former represents correctly a very large error, while the latter can be a reasonable assumption for centering errors of the order of a few mm.

The calculations have given an axial spring constant of ~ 1.5 Tons/mm and a radial one ~ 0.8 Tons/mm. Since it does not seem possible to extimate more accurately these forces large safety factors must be taken in designing the coils supports. The experience with the K-500 superconducting cyclotron at M. S. U. [7] has indicated in fact that positioning errors introduce not trivial forces since the measured radial spring constant resulted to be ~ 4 Tons/mm at the maximum coils excitation.

REFERENCES.

(1) - E. Acerbi et al., The Milan Superconducting Cyclotron Project, Proceedings of the IX Intern. Conf. on Cyclotrons and their Applications, Caen (France), 1981 (Les Editions de Physique, 1981), pag. 169.

(2) - E. Acerbi, F. Alessandria, G. Baccaglioni and L. Rossi, Design of the Main Coils for the Milan Superconducting Cyclotron, Proceedings of the IX Intern. Conf. on Cyclotrons and their Applications, Caen (France), 1981 (Les Editions de Physique, 1981), pag. 399.

(3) - R. F. Holsinger and C. Iselin, POISCR the CERN-Poisson program package, unpublished CERN Report.

(4) - G. Bellomo, D. A. Johnson, P. Miller and F. G. Resmini, Magnetic field mapping of the K-500 cyclotron, Nuclear Instr. and Meth. 180, 285 (1981).

(5) - E. Fabrici and F. G. Resmini, Poisson calculations for the Milan supeconducting cyclotron, to be published.

(6) - E. Acerbi, HERCULES code, stress calculations in superconducting coils, to be published.

(7) - P. Miller, private communication.